PHYSICAL REVIEW C VOLUME 13, NUMBER 1 JANUARY 1976

Perturbative approximations to the effective interaction: Comparisons with exact results for large matrices

S. Pittel
Bartol Research Foundation of The Franklin Institute, Swarthmore, Pennsylvania 19081

C. M. Vincent*
Department of Physics, University of Pittsburgh, Pittsburgh, Pennsylvania 15260

J. D. Vergados†
Department of Physics, University of Pennsylvania, Philadelphia, Pennsylvania 19174
(Received 29 September 1975)

The effective interaction appropriate to a $(2s\text{-}1d)^2$ model space is studied for the $J^\pi = 0^+$ states of ^{18}O. Perturbation theory and various Padé approximants are compared with exact results obtained by solving large shell-model problems that realistically include many 3p-1h and 4p-2h states. We analyze two cases that differ only in the choice of the $(2s\text{-}1d)$ single-particle energies. In one, there is a collective 4p-2h intruder state, as well as several intruders at negative values of the coupling parameter. The perturbation theory expansion for the effective interaction is found to diverge in this case. The other case has no intruders and the perturbation expansion seems to converge. In both cases, third-order perturbation theory is found to be more accurate than second order, and gives matrix elements correct to 200 keV. The intruder states do not seem to be responsible for the fact that third-order terms are often larger than second-order terms. The $[N+1, N]$ Padé approximants of low orders are less accurate than third-order perturbation theory. However, the operator-valued [1,2] Padé approximant is accurate to 130 keV, for reasons that are not yet understood.

[NUCLEAR STRUCTURE Effective interactions; tested perturbation theory and Padé approximants; ^{18}O $J^\pi = 0^+$ large-matrix calculations; included intruder states.]

I. INTRODUCTION

In this work we test various approximate methods for calculating the shell-model effective interaction,[1] by applying them to solvable test cases with realistic features. In particular, we investigate the accuracy of finite orders of perturbation theory (PT) as well as several related methods. Special attention is focused on a solvable large-matrix description of the $J^\pi = 0^+$ states of ^{18}O, in which a collective 4p-2h 0^+ state appears below the energy of the predominantly $(d_{3/2})^2$ state. The interest in this case derives from the prediction of Schucan and Weidenmüller[2] that PT for the effective interaction will diverge whenever such a low-lying collective "intruder" state exists.

The nuclear shell model aims to describe the simplest states of a given nucleus in terms of a *model space*, which is spanned by a few of the simplest available low-lying configurations. In principle, there exists an "effective" interaction[1] υ for use in the model space, such that υ implicitly takes account of configurations outside the model space and exactly reproduces the energies of the simplest states of the system. In practice, the computation of υ is a difficult dynamical problem, so that approximate methods must be used.

Perturbation theory is one of the best known and most widely used methods for discussing the effective interaction.[3,4] It has been formulated systematically[5-7] in terms of diagrams of the Feynman-Goldstone type, which are suitable for explicit computation of the various orders of PT. The diagrammatic expansion also lends itself to discussion of formal questions, such as the extent to which υ is a two-body operator. However, we are interested here in the accuracy of PT as an approximate technique of numerical calculation.

Because the bare two-nucleon interaction typically has a strongly repulsive core, PT can be applied only after the effects of the strong repulsion have been removed. The usual method is to express the bare interaction in terms of the Brueckner reaction matrix G[8] and expand the effective interaction υ in powers of G. In principle, the two phases of the calculation of υ must be done consistently to avoid double-counting problems.[9]

Early numerical studies of the renormalization of the G matrix in finite nuclei were carried out by Kuo and Brown.[10] They considered the effective interaction appropriate to a $(2s\text{-}1d)^2$ model space for the states of ^{18}O. Starting from a G

matrix calculated from a realistic (Hamada-Johnston) two-nucleon potential, they calculated corrections to it through second order in G. Their resulting matrix elements have been used with great success in nuclear structure studies in the $(2s\text{-}1d)$ shell.

Subsequently, Barrett and Kirson[11] extended the work of Kuo and Brown through third order in G, using the folded-diagram formulation of PT.[5] Their calculations were restricted to $J^\pi = 0^+$ states, but have since been extended by Goode[12] to other J^π states. The Barrett-Kirson study indicates that the third-order contributions to $\mathcal{V}$ are often larger than the second-order contributions. This result has stimulated the consideration of convergence properties of PT for the effective interaction.[2,13]

Conditions for mathematical convergence of PT expansions for $\mathcal{V}$ have been investigated by Schucan and Weidenmüller.[2] They conclude that PT should diverge whenever the perturbation is strong enough to depress an intruder state (composed mainly of configurations outside the model space) into the energy region occupied by the states that are predominantly in the model space. Since a 4p-2h intruder state is known[14] to exist in the 0^+ spectrum of ^{18}O, the ability of PT to approximate the effective interaction in this case is in doubt.

In response to the work of Schucan and Weidenmüller, many authors have suggested approximation schemes to use in the presence of intruder states. Many of these methods fall into the general category of "infinite partial summations."[15] A potentially promising method is the use of Padé approximants,[16,17] which, because of their close relation to PT, are amenable to systematic calculation. Padé approximants can either be used directly to approximate the effective interaction[16,17] or in conjunction with the Q-box formulation of PT.[18]

The various methods for approximating the effective interaction in the presence of intruder states were all developed with the hope that they may have larger domains of convergence than PT. However, convergence is not a necessary condition for a method to have practical value. As Vincent and Pittel have remarked,[19] the results obtained from low orders of a given approximation scheme may be of adequate accuracy, even though the scheme does not converge for infinitely high orders. In particular, they show that low orders of PT can sometimes provide good approximations, even though PT is divergent. In the present study, we therefore judge approximate methods by their accuracy in low orders, and not on the basis of mathematical convergence.

In the present paper, we study exactly solvable models constructed by replacing the infinite Hilbert space of the given nuclear system by a "large" space of finite dimensionality. Each solvable large-space problem will then correspond to a large (but finite) shell-model Hamiltonian matrix. It will be solvable only in the sense that the large Hamiltonian matrix can be diagonalized numerically, and not in the sense that a closed-form solution is known. This limits the size of the problems that can be considered but allows important realistic features to be incorporated. Thus, in our solvable description of the 0^+ states of ^{18}O, our large space includes not only the 2p-0h model-space states and some 3p-1h core-polarization states but also a fairly large number of 4p-2h states. The 4p-2h states generate the collectivity of the "deformed" intruder state. The "bare" interaction for the solvable problems is also chosen quite realistically.

In studying the accuracy of approximations, comparison with experiment is not appropriate. Instead, we use the "large-matrix" problems to generate exact results, which can be regarded as "data." The success of approximations ("theories") is then judged by comparison with these data. Comparison of the results for different large-matrix problems enables us to judge the range of validity of our conclusions.

It should be emphasized here that diagrammatic PT calculations also involve implicitly a large space, associated with the energy truncation of intermediate-state sums. The large-matrix approach to effective interactions makes the space truncation explicit, to facilitate comparison between exact and approximate results.

In Sec. II, we define the effective Hamiltonian $\mathcal{H}$ that is appropriate for representing a large-matrix problem in a model space. We also describe PT for $\mathcal{H}$, including convergence criteria and methods for calculating the orders of PT. Section III discusses calculation of the effective interaction $\mathcal{V}$ from $\mathcal{H}$, and extends to $\mathcal{V}$ the previous treatment of convergence criteria. Section IV describes three different types of Padé approximants that can be constructed for the matrix-valued effective interaction. In Sec. V, we discuss the solvable problems for which we test the various approximate methods. Section VI discusses the results of our calculations and obtains conclusions which are briefly summarized in Sec. VII.

II. EFFECTIVE HAMILTONIAN

A. Definitions and the construction of the effective Hamiltonian

Let H be the Hamiltonian for a given number of particles. We assume H to be an Hermitian oper-

ator acting in a large space spanned by the N orthonormal basis vectors $\{\phi_\alpha\}$, where $\alpha = 1, \ldots, N$. We shall discuss the reduction of this problem to a smaller space, called the *model space*. The model space is spanned by a basis containing $M < N$ of the states ϕ_α, chosen on physical grounds. We follow the convention that the states ϕ_α are labeled so that the first M span the model space. We define the *projection operator* P onto the model space by

$$P = \sum_{\alpha=1}^{M} |\phi_\alpha\rangle\langle\phi_\alpha| . \tag{1}$$

Similarly, the *excluded space* is defined as the space spanned by the remaining $N-M$ basis vectors. The projection onto the excluded space is

$$Q = \sum_{\alpha=M+1}^{N} |\phi_\alpha\rangle\langle\phi_\alpha| = 1 - P . \tag{2}$$

Denote the exact eigenvalues and eigenvectors of H by $\{E_\alpha\}$ and $\{\psi_\alpha\}$ and the projections of the ψ_α onto the model space by

$$\chi_\alpha \equiv P\psi_\alpha . \tag{3}$$

Of particular interest are those M wave functions ψ_α which have the largest possible components in the model space. We refer to this as the set of *predominantly model space states* and we denote this set of states by S.

In agreement with most authors, we define the *effective Hamiltonian* $\mathcal{H}$ as that operator on the model space whose eigenvalues and eigenvectors are E_α and χ_α for $\alpha \in S$. This definition specifies what is usually called the energy-independent effective Hamiltonian, as distinct from the energy-dependent effective Hamiltonian discussed by Bloch and Horowitz.[3]

The energy-independent effective Hamiltonian $\mathcal{H}$ is formally defined by the model-space Schrödinger equations

$$\mathcal{H}\chi_\alpha = E_\alpha\chi_\alpha \quad \text{for } \alpha \in S \tag{4}$$

and is given by[20,21]

$$\mathcal{H} = \sum_{\alpha \in S} |\chi_\alpha\rangle E_\alpha \langle\tilde{\chi}_\alpha| . \tag{5}$$

Here $\tilde{\chi}_\alpha$ belongs to the set $\{\tilde{\chi}_\alpha\}$ of vectors biorthonormal to the set $\{\chi_\alpha\}$, as defined by the relation

$$\langle\tilde{\chi}_\alpha|\chi_\beta\rangle = \delta_{\alpha\beta} \quad (\alpha, \beta \in S) . \tag{6}$$

The formula (5) for $\mathcal{H}$ has been used extensively in the literature.[20,21] Many other equivalent formulae are also known.[2]

As noted above, we shall always define $\mathcal{H}$ so as to reproduce the eigenvalues and eigenvectors of the predominantly model-space states. These are the states which the model-space Schrödinger equation would be expected to reproduce most faithfully. However, as pointed out by Schucan and Weidenmüller, this definition may lead to a discontinuous dependence of the eigenvalues E_α on the strength of the perturbation (see Sec. II B).

B. Perturbation theory for $\mathcal{H}$ and its convergence properties

We review here some results on the convergence of PT for the effective Hamiltonian. Much of this discussion follows Schucan and Weidenmüller.[2]

Let H_0 be a zero-order Hamiltonian whose eigenvalues and eigenvectors are known. Further, let us assume that the basis $\{\phi_\alpha\}$ is chosen to diagonalize H_0, so that

$$H_0\phi_\alpha = \epsilon_\alpha\phi_\alpha \quad (\alpha = 1, \ldots, N) . \tag{7}$$

We next define the perturbation

$$V \equiv H - H_0 \tag{8}$$

and construct an operator-valued function

$$H(z) = H_0 + zV , \tag{9}$$

which depends on a coupling parameter z. Clearly

$$H(0) = H_0$$

and

$$H(1) = H . \tag{10}$$

The value $z = 1$ is referred to as the "physical" value of z, since it gives rise to the physical Hamiltonian H. For each real z, Eqs. (9) and (5) define an energy-independent effective Hamiltonian $\mathcal{H}(z)$. Perturbation theory (PT) can be regarded as an expansion of $\mathcal{H}(z)$ in powers of z,

$$\mathcal{H}(z) = h_0 + zh_1 + z^2h_2 + \cdots . \tag{11}$$

Although $\mathcal{H}(z)$ has physical meaning only for $z = 1$, its convergence properties can conveniently be discussed by regarding it as an operator-valued function of a complex variable $z = x + iy$. Let z_0 be the singularity of $\mathcal{H}(z)$ that is nearest the origin. Then the series (11) converges at $z = 1$ if $|z_0| > 1$ and diverges at $z = 1$ if $|z_0| < 1$. The location of the singularities of $\mathcal{H}(z)$ is therefore important for convergence questions.

Schucan and Weidenmüller[2] state that the only singularities of $\mathcal{H}(z)$ are branch points at those points z_i in the complex plane for which the energy of a predominantly model-space state coincides with the energy of a predominantly excluded-space state. If any of these branch points lie within the unit circle, the series (11) diverges at $z = 1$.

Because the Hamiltonian $H(z)$ is Hermitian, the branch points always occur in complex conjugate

pairs. If two energy levels coincide at points $x_i \pm iy_i$ near the real axis, the energies as a function of real x come closest together for x near x_i. Although the levels will in general not coincide for any real x (the Wigner-von Neumann no-crossing rule), the two levels will exchange character as we go from $x < x_i$ to $x > x_i$. More specifically, if the predominantly model-space level is the lower (upper) level for $x < x_i$, it will be the upper (lower) level for $x > x_i$. In this spectroscopic sense, the levels are said to "cross" near $x = x_i$. It is customary to refer to a predominantly excluded-space state that penetrates the energy region of the model-space states as an *intruder state*. For such a pair of branch points, it is appropriate to draw a branch cut from $x_i + iy_i$ to $x_i - iy_i$.

Not all singularities of $\mathcal{K}$ correspond to "crossing" between intruder states and predominantly model-space states. Other singularities far from the real axis are, in principle, possible. However, for such singularities to occur within the unit circle, unphysically strong interaction between model- and excluded-space states would probably be required. For convergence questions, we can therefore confine our attention to crossing singularities.

C. Classification of intruder states

The kind of intruder state that is usually discussed in the literature corresponds to a crossing of a predominantly excluded-space state with a predominantly model-space state for positive x less than 1.[2,13] The presence of such intruder states can be recognized spectroscopically, since they intrude into the physical ($z = 1$) spectrum. We refer to an intruder state of this type as a *physical intruder state*, as shown in Fig. 1.

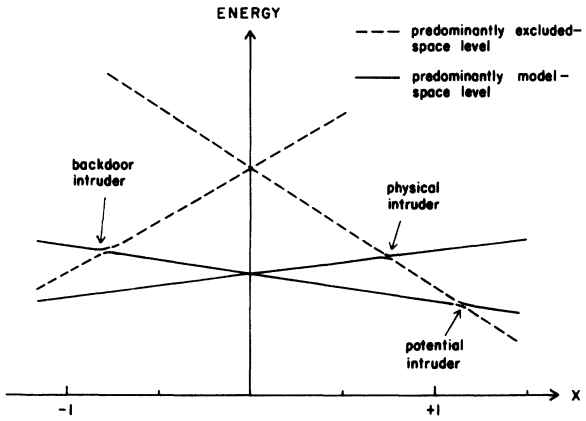

FIG. 1. A schematic illustration of the three types of intruder states that are discussed in this paper.

Kirson[22] uses the term *potential intruder* to describe crossings at x slightly greater than 1. Branch cuts associated with potential intruders do not cause the series (11) to diverge at $z = 1$, but may produce slow convergence. Potential intruders are expected to be important for the case of $J^\pi = 0^+$ states in ^{18}O and in many other cases as well.

We also illustrate in Fig. 1 a third class of intruder-state singularity, to which we refer as *backdoor intruders*. They result from a level crossing on the negative x axis, but within the unit circle. Unlike physical intruders, backdoor intruders cannot be recognized spectroscopically. However, even in the presence of a physical intruder, such a backdoor intruder may dominate high orders of PT if it is closer to the origin than any physical intruder-state singularity. This is the case for one of the calculations discussed in Sec. V.

D. Decomposition of $\mathcal{K}$

For later notational convenience, we introduce a decomposition of $\mathcal{K}(z)$ into a part $\mathcal{K}_{\rm reg}(z)$ that is regular within the unit circle and a part $\mathcal{K}_{\rm cut}(z)$ that has singularities within the unit circle only. A unique decomposition may be achieved by specifying that

$$\mathcal{K}_{\rm cut}(z) \to 0 \quad \text{as } z \to \infty \tag{12}$$

and that $\mathcal{K}_{\rm cut}(z)$ has the same cuts as $\mathcal{K}(z)$ inside the unit circle and the same discontinuity across each cut. Then the quantity $\mathcal{K}_{\rm reg}$ defined by

$$\mathcal{K} = \mathcal{K}_{\rm reg} + \mathcal{K}_{\rm cut} \tag{13}$$

is analytic inside the unit circle.

This decomposition is useful in discussing the errors of PT, since it allows the series to be separated into a convergent expansion for $\mathcal{K}_{\rm reg}$ and a divergent expansion for $\mathcal{K}_{\rm cut}$. Study of $\mathcal{K}_{\rm cut}$ allows one to assess the part of the error that is due to singularities within the unit circle.

E. Perturbation theory for $\mathcal{K}$

Lindgren[7] has recently described a PT expansion for $\mathcal{K}$ that applies even when the model space is not degenerate, that is when the zero-order energies $\epsilon_1 \ldots \epsilon_M$ [see Eq. (7)] are not equal. For completeness we present a brief discussion of his formulation.

The central ingredient is an operator Ω, called by Lindgren the wave operator and by others[23] the model operator. It is defined by

$$\Omega = \sum_{\alpha \in S} |\psi_\alpha\rangle\langle\tilde{\chi}_\alpha| , \tag{14}$$

and maps each model-space representation χ_α of a state onto the corresponding complete state ψ_α. Lindgren shows that the effective Hamiltonian and the wave operator are related by

$$\mathcal{H} = PH\Omega = PH_0P + PV\Omega \,. \tag{15}$$

Thus an expansion for $\mathcal{H}$ in powers of z can be obtained if an expansion of Ω is known. Denote this expansion by

$$\Omega(z) = \omega_0 + z\omega_1 + z^2\omega_2 + \cdots \,. \tag{16}$$

Lindgren derives the following recursion relation for the matrix elements of ω_n (for $n \geq 1$) in terms of the matrix elements of $\omega_0 \cdots \omega_{n-1}$:

$$\langle \phi_\alpha | \omega_n | \phi_\beta \rangle = \begin{cases} \dfrac{\langle \phi_\alpha | V\omega_{n-1} - \sum_{m=1}^{n} \omega_{n-m} V \omega_{m-1} | \phi_\beta \rangle}{\epsilon_\beta - \epsilon_\alpha} & (\alpha > M,\ \beta \leq M) \\ 0 \text{ otherwise} \,. \end{cases} \tag{17}$$

The calculation is started by setting

$$\omega_0 = P \tag{18}$$

and applying (17) as many times as desired. Finally, the PT expansion of $\mathcal{H}$ is calculated from

$$\begin{aligned} h_0 &= PH_0P \,, \\ h_n &= PV\omega_{n-1} \quad (n \geq 1) \,. \end{aligned} \tag{19}$$

The number of arithmetic operations required to compute $h_0, \ldots, h_n$ by this method for an N-dimensional large space and an M-dimensional model space (with $N \gg M$) is proportional to $M^2N^2n^2$. This rather slow dependence on n permits quite high orders of PT to be calculated.

F. Closed forms for low orders of PT

In the calculation of PT for $\mathcal{H}$, outlined in the previous section, each order h_n is evaluated as a whole, and no information is obtained about the individual many-body diagrams that contribute to h_n. However, some information on certain classes of diagrams can be obtained if one first derives explicit expressions for the various orders of PT, e.g., from the recursion relations (17).

We use a notation in which Latin subscripts refer to states in the model space and Greek subscripts to states in the excluded space. The terms of PT through fourth order are

$$(h_0)_{ij} = (H_0)_{ij} \,, \tag{20}$$

$$(h_1)_{ij} = V_{ij} \,, \tag{21}$$

$$(h_2)_{ij} = \sum_\alpha \frac{V_{i\alpha}V_{\alpha j}}{\epsilon_j - \epsilon_\alpha} \,, \tag{22}$$

$$h_3 = h_{3A} + h_{3B} \,, \tag{23}$$

where

$$(h_{3A})_{ij} = \sum_{\alpha,\beta} \frac{V_{i\alpha}V_{\alpha\beta}V_{\beta j}}{(\epsilon_j - \epsilon_\alpha)(\epsilon_j - \epsilon_\beta)} \,, \tag{24}$$

$$(h_{3B})_{ij} = -\sum_{\alpha,k} \frac{V_{i\alpha}V_{\alpha k}V_{kj}}{(\epsilon_j - \epsilon_\alpha)(\epsilon_k - \epsilon_\alpha)} \,, \tag{25}$$

$$h_4 = h_{4A} + h_{4B} + h_{4C} + h_{4D} \,, \tag{26}$$

where

$$(h_{4A})_{ij} = \sum_{\alpha,\beta,\gamma} \frac{V_{i\alpha}V_{\alpha\beta}V_{\beta\gamma}V_{\gamma j}}{(\epsilon_j - \epsilon_\alpha)(\epsilon_j - \epsilon_\beta)(\epsilon_j - \epsilon_\gamma)} \,, \tag{27}$$

$$(h_{4B})_{ij} = \sum_{\alpha,k,l} \frac{V_{i\alpha}V_{\alpha k}V_{kl}V_{lj}}{(\epsilon_j - \epsilon_\alpha)(\epsilon_k - \epsilon_\alpha)(\epsilon_l - \epsilon_\alpha)} \,, \tag{28}$$

$$(h_{4C})_{ij} = -\sum_{\alpha,\beta,k} \frac{V_{i\alpha}V_{\alpha k}V_{k\beta}V_{\beta j}}{(\epsilon_j - \epsilon_\alpha)(\epsilon_j - \epsilon_\beta)(\epsilon_k - \epsilon_\alpha)} \,, \tag{29}$$

$$(h_{4D})_{ij} = \sum_{\alpha,\beta,k} \frac{V_{i\alpha}V_{\alpha\beta}V_{\beta k}V_{kj}}{(\epsilon_j - \epsilon_\alpha)(\epsilon_j - \epsilon_\beta)} \times \left(\frac{1}{\epsilon_k - \epsilon_\alpha} + \frac{1}{\epsilon_k - \epsilon_\beta} \right) . \tag{30}$$

In these relations, doubly-subscripted quantities are matrix elements between basis states corresponding to the subscripts, e.g., $V_{ij} = \langle \phi_i | V | \phi_j \rangle$.

The various subterms in third and fourth orders can be pictorially represented as in Fig. 2. In this type of diagram, each state of the system is represented by a point and each action of V by a line. The arrows on these lines denote the transition of the system from each state to the next. Each diagram of this type is said to specify a *path* available to the system, in proceeding from a given initial state i to a given final state j. In these diagrams, all intermediate states are fully antisymmetric.

It is interesting to relate these paths to the usual diagrams of many-body theory, as discussed for example by Brandow.[5] The paths h_{3B}, h_{4C}, and h_{4D} are sums of once-folded diagrams and path h_{4B} is a sum of twice-folded diagrams. All other paths shown in Fig. 2 contain no folded diagrams.

The number of operations involved in evaluating an nth-order path using the above equations is greatest for "unfolded" paths, such as h_{3A}, which involve the maximum number of excluded intermediate states. The number of operations required to evaluate the unfolded nth-order path h_{nA}

is proportional to M^2N^{n-1} if $N \gg M$. This n dependence is much more rapid than that encountered for the recursive method. The recursive method already becomes far quicker by $n=4$. Nevertheless, since we feel it is worthwhile to know the contribution of individual paths, we calculate the terms of PT through $n=4$ in both ways.

III. EFFECTIVE INTERACTION

A. Construction of the effective interaction

The effective Hamiltonian discussed in Sec. II enters in any discussion of space truncation, independent of the specific nature of the problem. The basis states $\{\phi_\alpha\}$ and the related zero-order Hamiltonian H_0 could therefore be left unspecified. The concept of an *effective interaction,* however, requires careful consideration of the way in which the many-body features of the nuclear system are described in the nuclear shell model.

In what follows we will restrict our discussion to the effective interaction between two valence nucleons outside a closed-shell core. In principle, the effective interaction problem arises in a discussion of any number of nucleons outside a closed-shell core. However, if the shell model is to provide a practical microscopic theory of nuclear structure it is important that the effective interaction be predominantly a two-body operator, so that it can be calculated for the closed-shell-plus-two-valence-nucleon system and then applied directly to more complex systems.

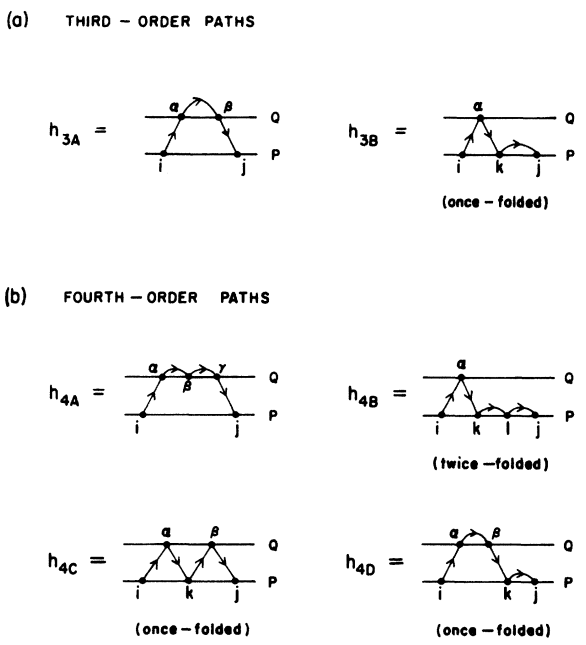

FIG. 2. Pictorial representation of the third-order and fourth-order paths that contribute to the PT series for the effective Hamiltonian $\mathcal{H}$.

An effective interaction v for two nucleons outside a closed-shell core can be constructed from the related effective Hamiltonian $\mathcal{H}$ by appropriately removing the core and single-particle contributions. The removal of these contributions requires the consideration of related large-matrix shell-model problems for the core and single-valence-particle nuclei, in addition to the two-valence-particle nucleus. It is important in this regard that the core and single-particle problems be constructed in appropriate analogy with the two-particle problem, in the sense of using the same many-body Hamiltonian and related basis states. We will spell these ideas out in greater detail in our specific examples of Sec. V.

The closed-core shell-model calculation provides as output the correlated energy $\bar{E}_c$ for the $J^\pi = 0^+$ ground state. The relevant states of the single-valence-nucleon $(c+1)$ system have various possible angular momenta, corresponding to the various possible active valence orbits. For each angular momentum j, a large-matrix shell-model problem can be constructed, the relevant output being the correlated energy $\bar{E}_{c+1}(j)$ of the predominantly single-particle state of angular momentum j. The effective single-particle energy $\bar{\epsilon}(j)$ for a nucleon in valence orbit j outside a correlated core is defined by

$$\bar{\epsilon}(j) = \bar{E}_{c+1}(j) - \bar{E}_c \,. \tag{31}$$

Similarly the two-valence-nucleon $(c+2)$ system is described by means of several large-matrix shell-model calculations, one for each J^π value. For each problem, the reduction from the large space to the model space gives rise to an effective Hamiltonian matrix $\langle\phi_\alpha|\mathcal{H}|\phi_\beta\rangle$, obtained according to (5).

The effective interaction matrix is defined by the relation

$$\langle\phi_\alpha|v|\phi_\beta\rangle = \langle\phi_\alpha|\mathcal{H}|\phi_\beta\rangle - \delta_{\alpha\beta}\{\bar{E}_c + \bar{\epsilon}(j_1) + \bar{\epsilon}(j_2)\}, \tag{32}$$

where j_1 and j_2 denote the two occupied valence orbits in ϕ_β. It can be constructed from the output of the large-matrix calculations using

$$\langle\phi_\alpha|v|\phi_\beta\rangle = \langle\phi_\alpha|\mathcal{H}|\phi_\beta\rangle + \delta_{\alpha\beta}\{\bar{E}_c - \bar{E}_{c+1}(j_1) - \bar{E}_{c+1}(j_2)\}. \tag{33}$$

It is useful to regard the core and single-valence-nucleon problems as effective Hamiltonian problems, each with a one-dimensional model space. In the closed-core problem, the model space consists of the state in which all core orbits

are completely filled (frequently called a 0p-0h state). Similarly each single-valence-nucleon problem involves a model-space state in which the core orbits are filled and the valence nucleon occupies a particular active orbit (called a 1p-0h state).

Each of the large-matrix problems involves the same many-body Hamiltonian and, consequently, each of the quantities appearing in (33) can be regarded as a function of the complex parameter z, introduced in Sec. II. Because the quantities $\tilde{E}_c$ and $\tilde{E}_{c+1}(j)$ can be viewed as effective Hamiltonians, the analysis of Sec. II C can be used to discuss their analytic properties and hence the analytic properties of $\mathcal{U}$.

B. PT for the effective interaction $\mathcal{U}$

The discussion of the PT for $\mathcal{U}$ follows easily from the results on PT for $\mathcal{H}$. We begin by considering the expansion of the operator $\mathcal{U}$ in powers of the coupling parameter z,

$$\mathcal{U}(z) = v_0 + v_1 z + v_2 z^2 + \cdots . \tag{34}$$

From (33) and the subsequent remarks, we see that $\mathcal{U}$ is a linear combination of the effective Hamiltonians for problems involving zero, one and two valence nucleons. It follows that the nth coefficient v_n in (34) can be written as

$$\langle \phi_\alpha | v_n | \phi_\beta \rangle = \langle \phi_\alpha | h_n | \phi_\beta \rangle + \delta_{\alpha\beta}\{ g_n^{(c)} - g_n^{(c+1)}(j_1) - g_n^{(c+1)}(j_2) \}, \tag{35}$$

where $g_n^{(c)}$ and $g_n^{(c+1)}(j)$ are the nth-order contributions to the core and single-particle effective Hamiltonians, respectively. We reserve the notation h_n for the nth-order contribution to the $(c+2)$-particle effective Hamiltonian. Each of the quantities h_n, $g_n^{(c)}$, and $g_n^{(c+1)}(j)$ can be computed using the recursion techniques of Sec. II D, for the appropriate large-matrix problem.

From (33) it also follows that $\mathcal{U}$ in general contains all the singularities of $\mathcal{H}$, $\tilde{E}_c$, and $\tilde{E}_{c+1}$. In analogy with the earlier decomposition of $\mathcal{H}$, we can decompose $\mathcal{U}$ in the form

$$\mathcal{U}(z) = \mathcal{U}_{\rm reg}(z) + \mathcal{U}_{\rm cut}(z) . \tag{36}$$

The quantity $\mathcal{U}_{\rm cut}(z)$ contains all the singularities of $\mathcal{U}$ within the unit circle. In most physical cases, the core and single-nucleon problems have no crossing singularities within the unit circle, so that

$$\mathcal{U}_{\rm cut}(z) = \mathcal{H}_{\rm cut}(z) . \tag{37}$$

The convergence properties of the PT series (34) follow immediately from these remarks about its singularities. We would normally expect that the PT expansion for $\mathcal{U}$ will diverge at $z = 1$ only if the two-valence-particle problem has intruder-state crossings within the unit circle.

Finally, we note that the contributions of individual paths to $\mathcal{U}$ can be calculated by appropriately combining the contributions of individual paths to $\mathcal{H}$, $\tilde{E}_c$, and $\tilde{E}_{c+1}(j)$.

C. Unlinked diagrams

Several authors[24-27] have remarked that the construction of an effective interaction $\mathcal{U}$ appropriate to a reduction from a large, but finite, space to a smaller model space involves unlinked diagrams. In contrast, the actual physical problem begins with an infinite and complete Hilbert space, so that these unlinked diagrams cancel. These remarks imply that "exact" effective interaction matrix elements derived from large-matrix calculations should not be compared with the partial sums of fully linked diagrammatic PT.

Within the framework of large-matrix studies of approximations to the effective interaction, there are two ways to insure that comparisons between PT results and exact results are meaningful. If one wishes to retain a linked PT expansion, then one must subtract the summed contribution of the unlinked diagrams from the exact $\mathcal{U}$. A method for making this correction has been given by Ellis.[26] Alternatively one can abandon the linked PT expansion and simply compare partial sums of the full power expansion of $\mathcal{U}$ for the finite large problem with the exact $\mathcal{U}$ for the same problem. We choose to follow the second approach, which is equally consistent.

Kirson[28] has remarked that the method of removing the unlinked diagrams from the exact $\mathcal{U}$ is preferable to the method we use, because it permits a more natural comparison with realistic diagrammatic PT results for $\mathcal{U}$. Because of the truncations spelled out in Sec. V, our model is admittedly not sufficiently realistic for a direct comparison with realistic PT calculations. Thus, we prefer to retain our simpler, but equally consistent, approach, and we believe that our con-

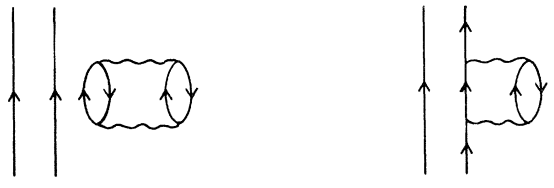

FIG. 3. Examples of unlinked diagrams that can contribute to the effective Hamiltonian $\mathcal{H}$ but are removed by the core and single-particle subtractions required in the effective interaction $\mathcal{U}$.

clusions regarding the applicability of approximation schemes will not be affected by this choice.

It should be noted that a large class of unlinked diagrams that can contribute to $\mathcal{K}$ are removed by the core and single-particle subtractions required in $\mathcal{U}$. For example, the core correction term $\tilde{E}_c$ serves to remove the "valence-spectator diagram" shown in Fig. 3(a). Similarly the single-particle correction terms $\tilde{E}_{c+1}(j)$ remove the unlinked diagram of Fig. 3(b). It is not until fourth order in the PT expansion of $\mathcal{U}$ that unlinked diagrams survive.[24]

IV. PADÉ APPROXIMANTS FOR $\mathcal{U}$

Padé approximants have recently been suggested as a possible scheme for extrapolating the effective interaction beyond its nearest intruder-state singularities.[16,17] Padé approximants attempt to simulate the singularities of a function by the poles and zeros of a rational function.

Let $F(z)$ be a function with power-series expansion

$$F(z) = \sum_{n=0}^{\infty} a_n z^n . \tag{38}$$

The $[K, L]$ Padé approximant to $F(z)$ is defined as the rational function

$$[K, L]F(z) \equiv R_K(z) S_L^{-1}(z) \tag{39}$$

whose power-series expansion agrees with (38) through the term in z^{K+L}. The polynomials R_K and S_L are of degrees K and L, respectively. Their coefficients are obtained by comparing the first $K+L+1$ powers of z in the equation

$$F(z) S_L(z) = R_K(z) \tag{40}$$

subject to the normalization condition $S_L(0) = 1$.

The interpretation of the above conditions for Padé approximants is somewhat different for scalar functions $F(z)$ than for operator-valued functions $F(z)$. For scalar functions, the inverse in (39) is interpreted as an ordinary scalar inverse, whereas for operator-valued functions it is interpreted as an operator inverse.

We shall not attempt to justify the use of Padé approximants. Much is known about the properties of Padé approximants to scalar functions,[29] including some general convergence criteria for functions with branch cuts.[30] Very little is known in the case of operator-valued functions. Our purpose will be simply to test the usefulness of Padé approximants for our exactly solvable and moderately realistic problems. Except for the work of Hofmann, Starkand, and Kirson[34] and of Starkand and Kirson,[35] Padé approximants to $\mathcal{U}$ have been studied only for very simple problems.

Several fairly general conclusions about Padé approximants have been suggested by earlier work on the subject. For example, because they have the correct behavior in the limit $x \to \infty$, the $[N+1, N]$ approximants to $\mathcal{U}(z)$ are expected to provide the best approximations.[16] It is also believed[16] that Padé approximants to $\mathcal{U}$ as an operator are preferable to Padé approximants to individual matrix elements of $\mathcal{U}$, particularly when the physical point $z = 1$ lies between strongly coupled branch cuts. We shall study the validity of these remarks within the framework of our solvable problems.

Besides the operator (OPADE) and matrix-element (MPADE) Padé approximants, we shall consider a form (TPADE) suggested by Lee and Pittel.[17] In the TPADE method, Padé approximants to individual matrix elements are calculated in a basis in which PHP is diagonal, and then transformed back to the original basis.

V. DESCRIPTION OF THE LARGE-MATRIX CALCULATIONS

A. Construction of large spaces for ^{16}O, ^{17}O, and ^{18}O

We shall consider, within the framework of the large-matrix approach, the effective interaction for two valence nucleons in a $J^\pi = 0^+$ state outside an ^{16}O core. More specifically, we shall consider a large space which includes

(a) the three possible $J^\pi = 0^+$ states obtained by distributing two valence nucleons in the $2s$-$1d$ shell, and
(b) all 3p-1h and 4p-2h states, subject to the restrictions that all holes are in the $1p_{1/2}$ orbit and only $2\hbar\omega$ excitations are permitted.

The model space will consist solely of the three states of two-particle (2p-0h) nature. The large space generated in this way contains 171 basis states, described in more detail in Table I.

As discussed in Sec. II, the choice of a large space and a model space (together with the choice of a Hamiltonian H) defines an effective Hamiltonian problem, which is solved according to (5). The construction of an effective interaction appropriate to this problem requires the introduction of auxiliary large-matrix problems for both the ^{16}O core nucleus and the ^{17}O single-particle nucleus. These auxiliary large-matrix problems must be chosen consistent with the basic ^{18}O large-matrix problem. We now discuss how this has to be done.

Our choice of a large space for the ^{18}O $J^\pi = 0^+$ problem is based on the following general restrictions:

(1) the active orbitals used are $1p_{1/2}$ (for holes) and $1d_{5/2}$, $2s_{1/2}$, $1d_{3/2}$, $1f_{7/2}$, $2p_{3/2}$, $1f_{5/2}$, $2p_{1/2}$ (for particles);

(2) at most two holes in the $1p_{1/2}$ hole orbit are allowed;

(3) up to $2\hbar\omega$ excitations, relative to the model-space states, are permitted.

We therefore subject our ^{16}O and ^{17}O large matrices to exactly the same restrictions. In the case of the ^{16}O $J^\pi = 0^+$ states, the model space is the 0p-0h closed-shell state. Three ^{17}O problems are required, corresponding to $J^\pi = \frac{5}{2}^+$, $\frac{1}{2}^+$, and $\frac{3}{2}^+$. In each, the model space consists of the single 1p-0h state of that angular momentum. The large spaces that we generate from the above restrictions are described in detail in Table II, for the various auxiliary problems.

Our ^{18}O $J^\pi = 0^+$ large space is rather different from that used by Lo Iudice, Rowe, and Wong.[20] They consider all orbits from $1s_{1/2}$ through the $1f$-$2p$ shell as active but restrict the basis to only 2p-0h and 3p-1h states. Because they use a larger set of active orbits, they are able to obtain a more realistic description of the core-polarization type of process than we can achieve. However, since our principal motivation is to use the large-matrix approach as a test of approximation schemes for υ in the presence of 4p-2h intruder states, we have included the 4p-2h configuration in our space. Our restriction of active orbits is unfortunately dictated by computational limitations.

Our omission of the $1p_{3/2}$-hole orbital requires discussion, since configurations involving two $1p_{3/2}$ holes probably play a large role in building up the collectivity that accounts for the low energy of the physical intruder state. This has two immediate consequences. First, the effective matrix elements derived from our calculations cannot be meaningfully compared either with experiment or with the results of diagrammatic calculations that permit intermediate excitations outside our space. Furthermore, since our space is not adequate to generate the full collectivity of the 4p-2h intruder state, it will be necessary to use some unphysical input to simulate a realistic intruder state.

TABLE I. ^{18}O $J^\pi = 0^+$ basis states.

	Type	Description	Number
P space	2p-0h	$(2s\text{-}1d)^2$	3
Q space	3p-1h	$(2s\text{-}1d)^2(2p\text{-}1f)1p_{1/2}^{-1}$	71
	4p-2h	$(2s\text{-}1d)^4(1p_{1/2})^{-2}$	97
		Total	171

B. Description of the single-particle and two-body input to the large space calculations

Having specified the configurations that enter in the large space calculations, it merely remains to specify

(a) the single-particle energies for all active orbits and
(b) a complete set of two-body matrix elements.

If we make the usual assumption that the two-body matrix elements refer to the same single-particle wave functions as do the single-particle energies, then the large-space shell-model calculation is completely defined.

We can associate the single-particle energies for all the active orbits with the eigenvalues of a Hartree-Fock Hamiltonian $H_0 = \sum_i h_0(i)$, for nucleons interacting with our chosen inert ^{16}O core. This Hamiltonian H_0 is used as the zero-order Hamiltonian in PT. In the calculations to follow, we shall assume two different (but related) sets of single-particle energies. The two choices are shown in Table III.

The first choice (denoted STD) is intended to simulate a fairly realistic set of single-particle energies, particularly for the important $2s$-$1d$ orbits. As a guide to choosing these energies, we have used the experimental spectra[31] of nuclei near ^{16}O. In a realistic calculation, one would not take the input single-particle energies from experiment, since the experimental energies include correlation effects of the kind we wish to consider. We neglect such problems of consistency, and assume that the energies in Table III (in the column denoted STD) are the eigenvalues of our zero-order Hamiltonian H_0.

The second choice (denoted DEG) is closely re-

TABLE II. Basis states for auxiliary ^{16}O and ^{17}O calculations.

		^{16}O $J^\pi = 0^+$		
	Type	Description	Number	
P space	0p-0h		1	
Q space	1p-1h	$2p_{1/2}1p_{1/2}^{-1}$	1	
	2p-2h	$(2s\text{-}1d)^2(1p_{1/2})^{-2}$	8	
		Total	10	

		^{17}O $J^\pi = \frac{5}{2}^+, \frac{1}{2}^+, \frac{3}{2}^+$			
			Number		
	Type	Description	$\frac{5}{2}^+$	$\frac{1}{2}^+$	$\frac{3}{2}^+$
P space	1p-0h	$(2s\text{-}1d)$	1	1	1
Q space	2p-1h	$(2s\text{-}1d)(1f\text{-}2p)1p_{1/2}^{-1}$	38	22	36
	3p-2h	$(2s\text{-}1d)^3(1p_{1/2})^{-2}$	92	53	86
		Totals	131	76	123

TABLE III. Single-particle energies for the STD and DEG calculations. All energies are given in MeV.

Case \ Orbital	$1p_{1/2}$	$1d_{5/2}$	$2s_{1/2}$	$1d_{3/2}$	$1f_{7/2}$	$2p_{3/2}$	$1f_{5/2}$	$2p_{1/2}$
STD	−10.670	−4.105	−3.280	0.960	8.830	8.830	8.830	8.830
DEG	−10.670	−2.302	−2.302	−2.302	8.830	8.830	8.830	8.830

lated to STD, except that we place the three orbits of the $2s$-$1d$ shell degenerate at the $(2J+1)$-weighted average energy of the corresponding STD levels. This choice is motivated by the fact that most diagrammatic calculations use degenerate energy denominators.

Both of the single-particle spectra we use have a major-shell gap of roughly 10 MeV. This is somewhat smaller than the 14-MeV gap that is usually considered appropriate for ^{16}O based on electron-scattering data. In the discussion of results in Sec. VI, we will see that a 10-MeV gap is needed to produce a physical intruder state. This reduced gap can be thought of as simulating the neglect of higher configurations (e.g. those with two holes in the $1p_{3/2}$ orbit), as discussed by Federman and Pittel.[32]

In both calculations STD and DEG, we use the same set of two-body interaction matrix elements, namely the bare G matrix elements of Kuo and Lee[33] calculated with a starting energy of −10 MeV.

In setting up exactly solvable, but moderately realistic, large-matrix problems, the use of bare G matrix elements is quite natural. For purposes of direct comparison with realistic PT calculations, we would no doubt want to choose these G matrix elements so as to avoid double-counting problems, perhaps by using Barrett's double-partition approach.[9] However, since for our purposes we require only qualitatively realistic input, the Kuo-Lee matrix elements seem adequate.

It is important to keep in mind that the full many-body Hamiltonians used in the STD and DEG calculations are not the same. Although both make use of the same perturbing interaction, they involve different zero-order Hamiltonians.

VI. RESULTS AND DISCUSSION

A. Standard (STD) case

For the nondegenerate single-particle spectrum [Fig. 4(a)] we obtain (for $z=1$) the ^{18}O $J^\pi=0^+$ spectrum shown in Fig. 4(b). The solid-line energy levels refer to the three predominantly model-space states. The dashed-line energy level at 10.53-MeV excitation energy is a physical intruder state, being 88% of 4p-2h character. Clearly this is not the correct location for the 4p-2h intruder. Experimentally, there is strong evidence that the first excited 0^+ state at 3.63 MeV is a predominantly 4p-2h intruder state.[14] Nevertheless, the present calculation does contain an intruder state with essentially the same 4p-2h character. Therefore it provides a suitable test of approximation schemes in the presence of an intruder state.

In Fig. 5, we show the calculated $J^\pi=0^+$ spectrum of ^{18}O as a function of the real coupling parameter x. The physical intruder state first penetrates the energy region of the model space for $x\approx 0.65$. In addition, there are several backdoor intruder-state crossings, in particular, one at $x=-0.251$. Clearly, for this calculation v_{cut}, the singular part of the effective interaction, contains contributions from several branch cuts within the unit circle.

The effective interaction matrix elements calculated for the STD case are shown in Table IV, in which the notation is also described. Here, v_n represents the nth-order term in PT, and P_n is the partial sum of the PT through nth order. The pair of integers (i,j) represents the labels of the basis states. The table shows the exact matrix elements of v as well as the values of P_n through ninth order. To facilitate judgments on the overall closeness of the approximation provided by P_n,

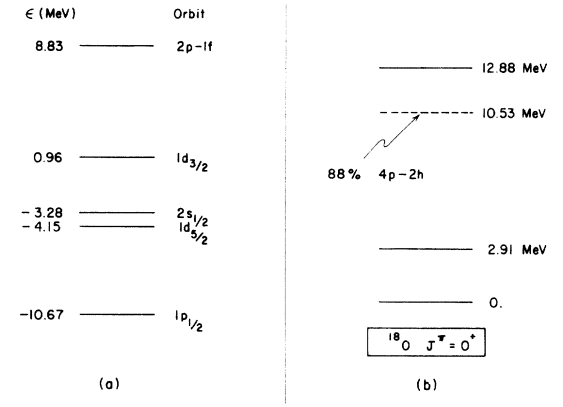

FIG. 4. The single-particle spectrum (a) and the resulting ^{18}O $J^\pi=0^+$ spectrum (b) for the STD case. A solid line in the calculated ^{18}O spectrum refers to a predominantly model-space state; a dashed line refers to a predominantly excluded-space state.

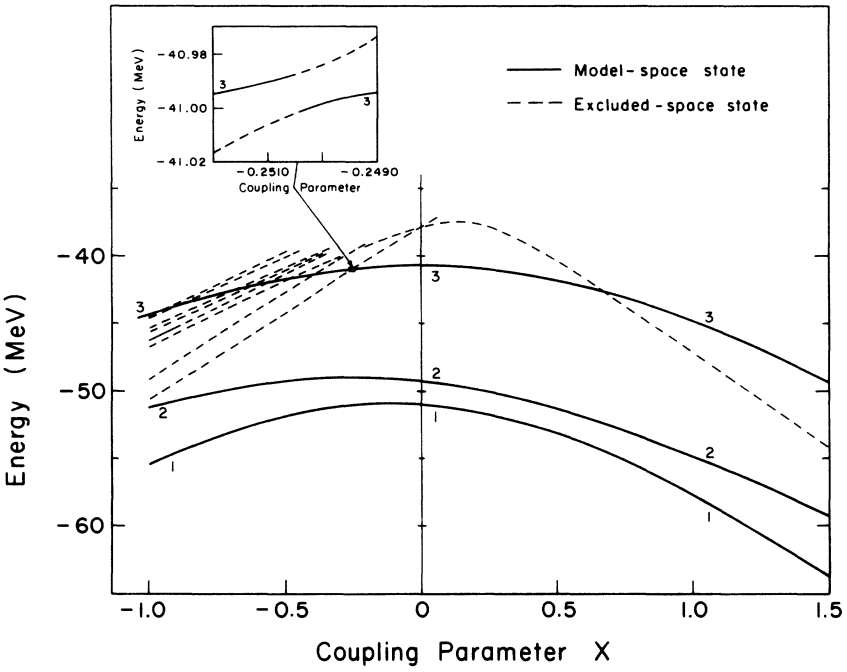

FIG. 5. Calculated ^{18}O $J^{\pi}=0^{+}$ energy spectrum for the STD case, as a function of the real coupling parameter x. The scale does not permit the noncrossing of levels to be shown. Less interesting portions of the spectrum are also not shown. The insert in the upper left shows an expanded view of the $x_c \approx -0.251$ backdoor intruder crossing.

we also show $\bar{e}_n$, the mean absolute discrepancy between the exact matrix elements of $\mathcal{U}$ and the nth-order approximate matrix elements P_n.

Perhaps the most dramatic feature of Table IV is the strongly divergent behavior of v_n at fairly high orders. By ninth order, the PT contribution to the (1, 3) matrix element of $\mathcal{U}$ is 180.352 MeV. This divergence must be attributed to one of the singularities within the unit circle, and its appearance already provides an interesting confirmation of Schucan and Weidenmüller's remark that PT diverges whenever there are intruder states.

Much can be inferred about the dominant intruder, by a more detailed analysis. According to

TABLE IV. Effective interaction matrix elements—STD case. Notation: $P_n=\sum_{m=1}^{n} v_m$, $\bar{e}_n=\frac{1}{9}\sum_{i,j}\left|\langle i|P_n|j\rangle-\langle i|\mathcal{U}|j\rangle\right|$, $1\equiv d_{5/2}^2$, $2\equiv 2_{1/2}^2$, $3\equiv d_{3/2}^2$. All results are given in MeV.

	1,1	2,1	3,1	1,2	2,2	3,2	1,3	2,3	3,3	$\bar{e}_n$
v_1	−1.346	−0.695	−3.162	−0.695	−2.171	−0.568	−3.162	−0.568	−0.055	
v_2	−0.736	−0.199	−0.119	−0.220	0.125	−0.033	−0.205	−0.051	0.073	
v_3	0.063	−0.033	0.382	−0.016	0.151	−0.016	0.844	−0.092	−0.256	
v_4	0.331	0.053	0.153	−0.071	0.069	−0.042	−0.998	−0.371	−0.027	
v_5	0.068	0.109	−0.168	0.065	−0.039	−0.014	1.708	−0.413	−0.197	
v_6	−0.626	0.086	−0.032	−0.130	−0.033	0.041	−4.121	0.327	0.351	
v_7	1.423	−0.128	0.007	0.346	0.008	−0.020	11.891	−0.159	−0.913	
v_8	−3.649	0.067	0.341	−0.979	0.049	0.056	−46.219	−0.248	2.273	
v_9	14.237	0.098	−0.798	3.553	−0.017	−0.195	180.352	−2.430	−9.357	
P_2	−2.082	−0.895	−3.281	−0.915	−2.046	−0.600	−3.367	−0.618	0.018	0.213
P_3	−2.018	−0.928	−2.899	−0.930	−1.895	−0.616	−2.524	−0.711	−0.238	0.054
P_4	−1.688	−0.875	−2.746	−1.001	−1.826	−0.658	−3.521	−1.081	−0.265	0.198
P_5	−1.620	−0.766	−2.914	−0.936	−1.865	−0.671	−1.813	−1.494	−0.462	0.260
P_6	−2.246	−0.680	−2.946	−1.067	−1.898	−0.631	−5.935	−1.168	−0.112	0.514
P_7	−0.823	−0.807	−2.939	−0.721	−1.890	−6.650	5.956	−1.326	−1.025	1.272
P_8	−4.472	−0.740	−2.598	−1.700	−1.841	−0.595	−40.262	−1.574	1.248	4.877
P_9	9.766	−0.642	−3.396	1.853	−1.858	−0.790	140.089	−4.005	−8.109	18.811
$\mathcal{U}$	−1.838	−0.897	−2.916	−0.989	−1.897	−0.652	−2.630	−0.691	−0.200	

Vincent and Pittel,[19] the contribution of a branch cut corresponding to a "crossing" at x_c is well represented by a pole at x_c, of the form

$$v_{\text{cut}}(z) = \frac{\mu}{z - x_c} \tag{41}$$

provided the length of the cut is much smaller than both $|x_c|$ and $|1 - x_c|$. At $z = 1$, the contribution of the cut to v_n is, therefore,

$$v_n(\text{cut}) = -\frac{\mu}{x_c^{n+1}} . \tag{42}$$

From the dependence of this result on x_c, it follows that the singularity with smallest $|x_c|$ (i.e., the one nearest the origin) dominates v_n for sufficiently large n, even if other singularities are stronger. This makes it possible to estimate the location of the dominant branch cut by comparing successive orders of PT. To a good approximation, the crossing closest to the origin occurs at

$$x_c \approx \frac{v_n}{v_{n+1}} \tag{43}$$

evaluated for sufficiently large n. By comparing v_8 and v_9 we see that

$$x_c \approx -0.25 . \tag{44}$$

Thus, in this case, the singularity that is nearest the origin corresponds to a backdoor intruder state (as can also be seen from Fig. 5) and not to a physical intruder state.

The residue μ of the pole in (41) must be matrix valued. For the crossing at $x_c = -0.251$, the matrix elements μ_{ij} are approximately given by

$$\mu_{ij} = -(x_c)^{10}(v_9)_{ij} , \tag{45}$$

since the cut dominates v_9. The possibility of calculating μ by means of (45) allows us to test the two-state model[19] of the residue. The Appendix outlines the model and discusses its numerical application to the singularity at $x_c = -0.251$. The results are very encouraging.

We note from Fig. 5 that there are several backdoor intruders in this calculation. All are predominantly very simple combinations of 4p-2h states, in contrast to the highly collective physical intruder state. The low energies of the backdoor intruders are primarily the result of strong particle-hole repulsion, which leads to large and positive diagonal matrix elements for these 4p-2h states. The physical intruder, in contrast, is lowered in energy by the strong interaction between the various 4p-2h states.

One might question whether backdoor intruders are likely to be present in more realistic calculations. Since the energies of these states are dominated by their diagonal interaction matrix elements, the amount by which the perturbation depresses them (roughly 9 MeV for the lowest) would probably not be increased much if a larger space were used. As noted earlier, a larger-space calculation would use a larger particle-hole gap. By estimating the energy of the lowest excluded states that would be expected at $z = -1$ for a gap of 14 MeV, we conclude that backdoor intruders are a real possibility in more realistic calculations. However, they would probably be much further from the origin than they are in the present calculation.

A second point to note in Table IV is that third-order PT (P_3) provides the best over-all fit to the exact $\mathcal{U}$, the mean absolute discrepancy being only 0.054 MeV.

Finally, we note that the third-order contributions v_3 to the (3, 1), (1, 3), and (3, 3) matrix elements of $\mathcal{U}$ are significantly larger than the associated second-order contributions v_2. This same feature was first noted in the realistic folded-diagram calculations of Barrett and Kirson[11] and has provided much of the motivation for studying the convergence of $\mathcal{U}$. Nevertheless, for all of these matrix elements, adding in the third-order contribution improves the agreement with the exact results.

B. Degenerate (DEG) case

For the degenerate single-particle spectrum [Fig. 6(a)], we obtain for $z = 1$ the ^{18}O $J^\pi = 0^+$ spectrum shown in Fig. 6(b). Here, the three lowest calculated states are predominantly model-space states, and the spectrum exhibits no intruder. A similar calculation at $z = -1$ also shows no signs of a backdoor intruder. In the STD calculation,

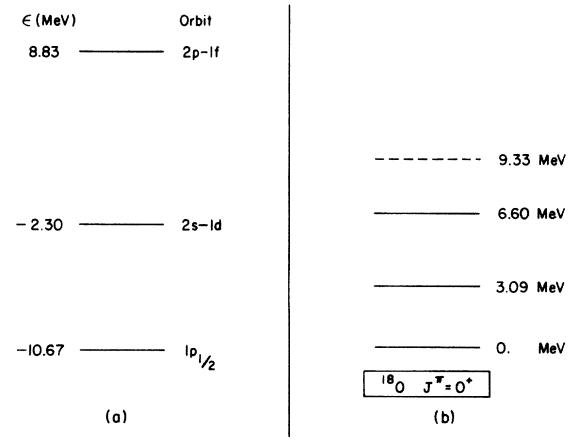

FIG. 6. The single-particle spectrum (a) and the resulting ^{18}O $J^\pi = 0^+$ spectrum (b) for the DEG case. Solid and dashed energy levels in (b) have the same meaning as in Fig. 4.

intruders occur primarily because of the large zero-order excitation energy of the $d_{3/2}{}^2$ basis state. In the DEG calculation, the $d_{3/2}{}^2$ state is degenerate in zero order with the other model-space states and, consequently, no intruders appear. Thus, in spite of the similarities of the two calculations, the analytic structure of the associated effective interactions are very different, since one calculation permits intruder states and the other does not. *A priori*, one might guess that PT would behave very differently in the two calculations.

The effective interaction matrix elements for the DEG case are shown in Table V. The table shows both the exact matrix elements of $\mathcal{U}$ and the PT matrix elements through ninth order. Here, we see from the mean discrepancies that the series seems to converge, though rather slowly. About seven terms are required to stabilize the results to a mean discrepancy of 0.014 MeV, after which the error is slowly reduced by adding higher orders.

While the addition of higher orders certainly improves the over-all agreement with the exact matrix elements, a reasonable approximation is obtained as early as third order, for which the mean discrepancy is 0.056 MeV.

It is instructive to note that the usual folded-diagram calculations of $\mathcal{U}$ replace the Hartree-Fock energy denominators by simple $n\hbar\omega$ energy denominators. These calculations are therefore more closely related to our DEG calculation than to our STD calculation. Our results suggest that the use of degenerate PT in realistic calculations can dramatically change the character of the problem, from a problem with intruder states and a divergent PT expansion to one which may not have an intruder state and may therefore have a convergent PT expansion.

C. Comparison of STD and DEG cases

It is of interest to compare directly the results of the STD and DEG calculations, to see more clearly the influence of intruder-state singularities within the unit circle.

The first feature that emerges from this comparison is that, through third order, PT exhibits a very similar behavior in the two calculations. In particular, the same matrix elements for which the STD calculation predicts large third-order contributions (i.e., large values of v_3) are also found to have large third-order contributions in the DEG calculation. These results suggest that the existence of third-order contributions that are large compared to the associated second-order contributions is unrelated to the intruder-state phenomenon. It seems reasonable to conclude that the same remarks apply to the more realistic calculations of Barrett and Kirson,[11] namely, that the large third-order contributions that they calculate are also unrelated to intruder-state singularities. This same conclusion has been reached by considering the contributions of specific 4p-2h

TABLE V. Effective interaction matrix elements—DEG case. Notation: $P_n=\sum_{m=1}^{n} v_m$, $\bar{e}_n=\frac{1}{9}\sum_{i,j}\left|\langle i|P_n|j\rangle-\langle i|\mathcal{U}|j\rangle\right|$, $1\equiv d_{5/2}{}^2$, $2\equiv 2_{1/2}{}^2$, $3\equiv d_{3/2}{}^2$. All results are given in MeV.

	1,1	2,1	3,1	1,2	2,2	3,2	1,3	2,3	3,3	$\bar{e}_n$
v_1	−1.346	−0.695	−3.162	−0.695	−2.171	−0.568	−3.162	−0.568	−0.055	
v_2	−0.679	−0.202	−0.154	−0.202	0.126	−0.040	−0.154	−0.040	0.072	
v_3	0.044	−0.041	0.390	0.005	0.141	−0.034	0.554	−0.012	−0.151	
v_4	0.415	0.005	0.138	−0.054	0.068	−0.048	−0.022	−0.034	−0.038	
v_5	−0.177	0.021	−0.157	−0.020	−0.037	−0.013	−0.146	0.005	0.022	
v_6	−0.059	−0.010	−0.082	0.013	−0.035	0.025	0.060	0.023	0.021	
v_7	0.021	−0.032	0.071	0.002	0.018	0.006	0.095	0.013	0.006	
v_8	0.089	−0.003	0.042	−0.014	0.013	−0.016	−0.042	0.009	0.006	
v_9	−0.068	0.016	−0.043	0.005	−0.011	−0.006	−0.030	0.002	−0.006	
P_2	−2.025	−0.898	−3.315	−0.898	−2.045	−0.608	−3.315	−0.608	0.017	0.183
P_3	−1.981	−0.939	−2.926	−0.893	−1.904	−0.642	−2.761	−0.620	−0.134	0.056
P_4	−1.566	−0.934	−2.787	−0.946	−1.837	−0.690	−2.783	−0.654	−0.173	0.063
P_5	−1.743	−0.913	−2.944	−0.966	−1.874	−0.703	−2.929	−0.649	−0.151	0.034
P_6	−1.803	−0.924	−3.026	−0.953	−1.909	−0.677	−2.869	−0.626	−0.129	0.033
P_7	−1.782	−0.956	−2.955	−0.951	−1.890	−0.672	−2.774	−0.614	−0.124	0.014
P_8	−1.693	−0.959	−2.913	−0.965	−1.878	−0.688	−2.816	−0.605	−0.118	0.014
P_9	−1.762	−0.944	−2.956	−0.960	−1.889	−0.693	−2.847	−0.603	−0.123	0.010
$\mathcal{U}$	−1.736	−0.955	−2.960	−0.958	−1.889	−0.685	−2.811	−0.599	−0.120	

TABLE VI. Third-order path contributions.

	1,1	2,1	3,1	1,2	2,2	3,2	1,3	2,3	3,3
					STD case				
v_{3A}	−0.362	−0.222	−0.281	−0.275	−0.443	−0.150	−1.993	−0.521	−0.304
v_{3B}	0.426	0.189	0.663	0.259	0.593	0.133	2.837	0.428	0.048
v_3	0.063	−0.033	0.382	−0.016	0.151	−0.016	0.844	0.092	−0.256
					DEG case				
v_{3A}	−0.362	−0.215	−0.328	−0.215	−0.346	−0.171	−0.328	−0.171	−0.190
v_{3B}	0.406	0.174	0.718	0.220	0.486	0.137	0.882	0.159	0.039
v_3	0.044	−0.041	0.390	0.005	0.141	−0.034	0.554	−0.012	−0.151

intermediate states to diagrammatic PT calculations.[36]

To illustrate more clearly the extent to which the two calculations STD and DEG are related through third order, we show in Table VI the contributions of the individual third-order paths v_{3A} and v_{3B}, as described in Sec. II F. As a reminder, the path v_{3A} corresponds to a sum of third-order unfolded diagrams and the path v_{3B} to a sum of third-order folded diagrams. The tendency of v_{3A} and v_{3B} to cancel is very strong. For the matrix elements (3, 1) and (3, 3), the behavior of v_{3A} and v_{3B} is very similar for the STD and DEG cases. For the matrix element (1, 3), however, the situation is more complicated. Although both v_{3A} and v_{3B} are individually much larger in the STD case than in the DEG case, their cancellation is still so close that the net value of v_3 is about the same for the two cases.

A careful comparison of Tables IV and V suggests that the intruder state singularities of the STD case might first be contributing importantly in fourth order, as reflected in the largeness of the (1, 3) and (2, 3) matrix elements of v_4 in the STD case as compared to the DEG case. The effect shows up even more dramatically in higher orders.

In Table VII, we show the decomposition of v_4 into individual paths, for both the STD and DEG cases. The tendency for the unfolded path v_{4A} to cancel the folded path v_{4D} is striking. The paths v_{4B} and v_{4C} are usually rather smaller and also tend to cancel each other. In the STD case, the (1, 3) matrix element of v_4 seems to be large mainly because v_{4A} and $v_{4\Gamma}$ are both large and do not cancel perfectly. In the DEG case, however, both v_{4A} and v_{4D} are small and the total v_4 is also small.

To understand the large values for the (1, 3) matrix elements of v_{4A} and v_{4D}, we have studied the contributions from specific sets of intermediate states, i.e., from individual terms in (27) and (30). We find that very few terms make sizable contributions to v_{4A} and v_{4D}. All terms of importance have excluded intermediate states

$$\alpha = \beta = [1d_{5/2}{}^4(J_1 = 0)1p_{1/2}{}^{-2}(J_2 = 0)]^{J=0} .$$

As noted earlier, the diagonal matrix elements associated with such states are often large and positive because of the strong repulsion between

TABLE VII. Fourth-order path contributions.

	1,1	2,1	3,1	1,2	2,2	3,2	1,3	2,3	3,3
					STD case				
v_{4A}	0.016	−0.117	0.020	−0.152	−0.024	−0.097	2.341	−0.869	−0.649
v_{4B}	−0.636	−0.118	−0.046	−0.178	−0.106	−0.034	−0.327	−0.144	−0.153
v_{4C}	0.485	0.102	0.050	0.128	0.050	0.014	0.259	0.053	0.218
v_{4D}	0.466	0.185	0.130	0.132	0.149	0.076	−3.271	0.583	0.557
v_4	0.331	0.053	0.153	−0.071	0.069	−0.042	−0.998	−0.371	−0.027
					DEG case				
v_{4A}	−0.035	−0.157	−0.033	−0.157	−0.049	−0.106	−0.033	−0.106	−0.126
v_{4B}	−0.190	−0.059	−0.066	−0.069	−0.069	−0.045	−0.079	−0.046	−0.131
v_{4C}	0.502	0.099	0.077	0.099	0.065	0.019	0.076	0.019	0.084
v_{4D}	0.138	0.121	0.160	0.072	0.121	0.085	0.014	0.099	0.134
v_4	0.415	0.005	0.138	−0.054	0.068	−0.048	−0.022	−0.034	−0.038

particles and holes. These states are also low in zero-order energy, so that the appropriate energy denominators are small. The same large diagonal matrix elements are also responsible for the existence of backdoor intruders. Thus, we conclude that the large fourth-order effects in the STD calculation are largely a reflection of backdoor intruder-state singularities.

It seems likely that the approximate cancellation of paths exhibited in Tables VI and VII is closely related to the approximate cancellation of diagrams belonging to number-conserving sets.[37]

In both the STD and DEG calculations, the partial summations of PT through third order (P_3) provide an excellent approximation to the exact $\mathcal{U}$. This suggests that in carrying out realistic PT calculations, in which it is not known *a priori* whether an intruder state exists, one can obtain a reasonably good effective interaction by carrying out a partial summation through third order. Of course, we have verified this conclusion only for the calculations reported here. In calculations involving potential intruders near $x=1$, it is possible that the convergence of $\mathcal{U}_{\text{reg}}$ will be so slow that P_3 is not adequate. Nevertheless, the possibility that P_3 may, in general, be a useful approximation to $\mathcal{U}$ is very encouraging, since diagrammatic PT calculations may never be computationally feasible beyond third order. For this reason, we are planning future calculations in which the single-particle spectra will not lead to situations that are as favorable for low-order PT as in the present calculations. In particular, we would like to study approximations to $\mathcal{U}$ under circumstances in which a physical crossing takes place barely inside the unit circle and in which a potential crossing takes place just outside the unit circle. The consideration of such less-favorable cases is essential to test the general validity of the above conclusions, so that they can be used reliably in full-scale realistic diagrammatic calculations.

D. Padé approximants

The PT results for the STD case exhibit a strong divergence associated with branch-cut singularities within the unit circle. It is of interest to see whether Padé approximants (PA) can be used to extrapolate $\mathcal{U}$ to the physical point $z=1$. Table VIII shows the $[N+1,N]$ Padé approximants to $\mathcal{U}$ for the STD case. As noted in Sec. IV these are expected to be the most useful Padé approximants. We include the three classes of Padé approximants introduced in Sec. IV, namely OPADE, MPADE, and TPADE. The exact matrix of $\mathcal{U}$ as well as the matrix elements of P_3 are included to facilitate comparison. We use here the symbol $\bar{e}$ to denote the mean absolute deviation of a given approximation from the exact effective-interaction matrix.

Note that all three of the calculated [2, 1] approximants are in poor agreement with $\mathcal{U}$, particularly in comparison with P_3, which also includes information through third order in PT. Several of the higher-order $[N+1,N]$ approximants give better approximations to $\mathcal{U}$, most notably the [4, 3]

TABLE VIII. $[N+1,N]$ Padé approximants—STD case. Notation: $\bar{e}=\frac{1}{9}\sum_{i,j}\left|\langle i\,|\mathcal{U}_{\text{approx}}|j\rangle-\langle i\,|\,\mathcal{U}\,|j\rangle\right|$.

	1,1	2,1	3,1	1,2	2,2	3,2	1,3	2,3	3,3	$\bar{e}$
					MPADE					
[2,1]	−2.023	−0.934	−3.190	−0.932	−2.776	−0.633	−3.202	−0.506	−0.039	0.263
[3,2]	−1.752	−1.335	−2.938	−0.978	−1.959	−0.239	−2.759	−0.539	4.047	0.573
[4,3]	−1.817	−0.947	−2.910	−0.981	−1.881	−0.668	−2.948	−0.337	−0.394	0.109
[5,4]	−1.818	−0.780	−2.779	−0.983	−1.863	−0.646	−2.800	5.186	−0.393	0.575
					OPADE					
[2,1]	−3.008	0.808	−3.489	0.495	−3.897	−0.263	−3.755	0.147	−0.172	0.712
[3,2]	−1.852	−0.755	−3.001	−0.808	−2.103	−0.572	−3.207	−0.562	−0.077	0.171
[4,3]	−1.783	−0.792	−2.872	−0.974	−1.858	−0.638	−2.996	−1.264	−0.471	0.165
[5,4]	−1.732	−0.649	−2.816	−0.959	−1.845	−0.632	−3.261	−1.798	−0.651	0.305
					TPADE					
[2,1]	−2.654	−0.594	−3.085	−0.551	−3.211	−0.199	−3.069	0.117	−0.655	0.551
[3,2]	−1.877	−0.465	−3.102	−1.079	−3.745	−0.622	−2.985	0.530	−0.907	0.428
[4,3]	−1.793	−0.524	−2.983	−0.754	−3.250	−0.210	−2.932	0.093	−0.705	0.436
[5,4]	−1.951	−0.662	−2.525	−1.615	−1.443	−2.719	−3.268	−0.089	1.715	0.738
P_3	−2.018	−0.928	−2.899	−0.930	−1.895	−0.616	−2.524	−0.711	−0.238	0.054
$\mathcal{U}$	−1.838	−0.897	−2.916	−0.989	−1.897	−0.652	−2.630	−0.691	−0.200	

TABLE IX. $[N+1,N]$ Padé approximants—DEG case.

	1,1	2,1	3,1	1,2	2,2	3,2	1,3	2,3	3,3	$\bar{e}$
					MPADE					
[2,1]	−1.984	−0.950	−3.205	−0.893	−3.195	−0.836	−3.195	−0.625	−0.032	0.280
[3,2]	−1.787	−1.035	−2.958	−1.050	−1.991	−6.798	−2.885	−0.711	−0.144	0.739
[4,3]	−1.759	−0.931	−2.987	−0.955	−1.881	−0.692	−2.908	−0.630	−0.129	0.025
[5,4]	−1.712	−0.925	−2.951	−0.959	−1.888	−0.685	−2.817	−0.616	−0.115	0.010
					OPADE					
[2,1]	0.700	−4.219	−2.303	−4.096	2.384	−1.787	−2.353	−1.725	0.272	1.872
[3,2]	−1.971	−0.732	−3.023	−0.721	−2.112	−0.579	−2.939	−0.570	−0.168	0.144
[4,3]	−1.740	−0.933	−2.946	−0.949	−1.877	−0.686	−2.873	−0.636	−0.138	0.020
[5,4]	−1.744	−0.940	−2.949	−0.951	−1.890	−0.685	−2.856	−0.603	−0.121	0.010
					TPADE					
[2,1]	−1.933	−0.692	−3.382	−0.663	−2.630	−0.446	−3.207	−0.418	0.143	0.333
[3,2]	−1.825	−0.835	−2.971	−0.829	−2.118	−0.597	−2.908	−0.575	−0.158	0.092
[4,3]	−1.739	−0.928	−2.961	−0.972	−1.884	−0.659	−2.852	−0.638	−0.152	0.021
[5,4]	−1.882	−1.001	−3.076	−1.013	−1.907	−0.686	−2.756	−0.608	−0.082	0.054
P_3	−1.981	−0.939	−2.926	−0.893	−1.904	−0.642	−2.761	−0.620	−0.134	0.056
$\mathcal{V}$	−1.736	−0.955	−2.960	−0.958	−1.889	−0.685	−2.811	−0.599	−0.120	

MPADE and OPADE.

Further information is obtained by studying the dependence of the Padé approximants on the real coupling parameter x. Rapid variations with x are associated with PA poles on the real axis. In these calculations, the locations of the PA poles seem to change from order to order and have no obvious connection with intruder-state singularities. Rather generally, we find that a PA will not be good whenever it has a pole near $z=1$. For example, the [3, 2] and [5, 4] MPADE approximants and the [2, 1] and [5, 4] OPADE approximants all have poles fairly near $z=1$ and, consequently, provide poor approximations to $\mathcal{V}$. If we disregard those orders for which poles are known to occur near $z=1$, the $[N+1,N]$ OPADE and MPADE approximants seem to be converging, albeit rather slowly.

In Table IX, we show the $[N+1,N]$ Padé approximants calculated for the DEG case. As in the STD case, the [2, 1] approximants are in poor agreement with $\mathcal{V}$. This is not surprising, since the PT results for the two cases are very similar through third order. The higher-order PA provide good over-all reproduction of $\mathcal{V}$, although usually not quite as good as the partial sum of PT through the same order as is used to generate the approximant.

We have calculated other $[N,M]$ Padé approximants to $\mathcal{V}$ for the two cases under discussion. In general, the $[N+1,N]$ approximants provide the best over-all agreement with $\mathcal{V}$, with one dramatic exception. The exception is the [1, 2] approximant, for which we show the OPADE results for the STD and DEG cases in Table X. In both cases, the results are in remarkable agreement with $\mathcal{V}$, the mean absolute discrepancies being only 0.040 and 0.045 MeV, respectively. These mean discrepancies are even smaller than those associated with P_3 for the two calculations. The [1, 2] MPADE approximant also provides an excellent fit to $\mathcal{V}$ ($\bar{e}=0.037$ MeV) in the DEG case, but a noticeably worse fit to $\mathcal{V}$ ($\bar{e}=0.076$ MeV) in the STD case. We do not yet understand why the [1, 2] operator Padé approximant works so well.

In general, our Padé calculations support the

TABLE X. [1, 2] OPADE results—STD and DEG cases.

	1,1	2,1	3,1	1,2	2,2	3,2	1,3	2,3	3,3	$\bar{e}$
STD	−1.812	−0.899	−2.966	−0.865	−1.935	−0.617	−2.683	−0.670	−0.206	0.040
DEG	−1.822	−0.898	−2.970	−0.855	−1.938	−0.631	−2.834	−0.609	−0.131	0.045

conclusions recently reported by Hofmann, Starkand, and Kirson.[34] To obtain satisfactory accuracy with the $[N+1,N]$ approximants requires about seven orders of PT. A similar level of accuracy can be obtained, at least for the calculations reported here, by summing PT through third order. Even if the presence of strong potential intruders in more realistic calculations should destroy the usefulness of P_3, it is doubtful that the PT calculations can ever by carried out to sufficiently high order to make the $[N+1,N]$ Padé approximants a viable alternative. The [1, 2] operator Padé approximant, however, requires only three orders of PT for its construction. Thus, if this Padé approximant can be shown to remain reliable in the presence of strong potential intruders, it could perhaps be a particularly useful means of approximating the effective interaction.

VII. CONCLUSIONS

We summarize here the principal conclusions that we have drawn from this study.

(1) The singularities of the realistic effective interaction are not restricted to physical intruder-state singularities. Backdoor intruder states are also a real possibility.

(2) Even when intruder states are present, the PT series for $\hat{U}$ seems to have a quasiasymptotic property, third order (P_3) providing the best approximation.

(3) The third order of PT is often larger than the second order. This does not seem to be due to intruders. In general, the inclusion of these large third-order contributions improves the approximation.

(4) The $[N+1,N]$ Padé approximants do not reliably provide better approximations to $\hat{U}$ than PT if only low orders are available.

(5) The [1, 2] operator Padé approximant provides the best approximation to $\hat{U}$ if only information through third order in PT is available. The excellence of this approximation warrants further understanding.

(6) The Vincent-Pittel two-state method (when extended to a multidimensional model space) seems to be quite successful in estimating the strengths of crossing singularities.

(7) Diagrammatic calculations of $\hat{U}$ that use degenerate ($n\hbar\omega$) energy denominators may lead to an effective interaction with a very different analytic structure than the "true" effective interaction.

(8) The best accuracy attainable with the approximations we have tested is probably about 200 keV. This may be adequate for some purposes, but will probably impose limitations on the applicability of $\hat{U}$ to more complex systems far from closed shells.

VIII. ACKNOWLEDGMENTS

A preliminary report of this work was presented at the International Topical Conference on Effective Interactions and Operators held at the University of Arizona in June 1975. Much of the discussion in this paper reflects ideas generated at this conference. We are grateful to the many conference participants with whom we had the opportunity to discuss effective interactions, particularly Michael Kirson, Bruce Barrett, Nicola Lo Iudice, and S. Y. Lee.

We would like to thank Joe McGrory for supplying us with a version of the Oak Ridge-Rochester shell-model code and Tom Kuo for sending us the two-body matrix elements used in this investigation. One of the authors (S.P.) would also like to acknowledge several helpful discussions with Harry Lee. We also wish to thank Michael Kirson for pointing out several errors in Tables VIII and IX of the manuscript.

APPENDIX

An extended form of the Vincent-Pittel two-state model of the residue μ of a branch cut suggests that μ is a separable operator. For the trace of μ, the extended two-state model predicts the form

$$\mathrm{tr}\mu = \frac{m^2 x_c^{\,2}}{d} \tag{A1}$$

which is the same as the scalar residue given by the original two-state model.[19] In this equation, m is the matrix element of V between the eigenvectors of PHP and QHQ that correspond to the levels that "cross" at x_c, and d is the relative x derivative of these two energies at x_c (and of the same sign as x_c).

The separable operator μ that results from the extended two-state model is either positive or negative semidefinite, so that $|\mathrm{tr}\mu|$ (A1) gives an upper bound on its single nonzero eigenvalue (which is real). However, μ is not Hermitian and may have matrix elements that are larger than all its eigenvalues.

For the singularity at $x_c = -0.251$, discussed in Sec. VI A, we find by applying (45) to the matrix elements of v_0 in Table IV that

$$\mathrm{tr}\mu = -4.76\times10^{-6}\ \mathrm{MeV}\,. \tag{A2}$$

The following values of mx_c and d are obtained by diagonalizing H in the neighborhood of $z = -0.251$:

$$\begin{aligned} mx_c &= -0.0082\ \mathrm{MeV}\,, \\ d &\approx -10\ \mathrm{MeV}\,. \end{aligned} \tag{A3}$$

Inserting these values into (A1), we obtain

$$\mathrm{tr}\mu = -6.72\times10^{-6}\ \mathrm{MeV}, \tag{A4}$$

in good qualitative agreement with (A2).

We have also investigated the prediction for the minimum separation E_{gap} between the crossing levels for real x. From the insert in Fig. 5, we find

$$E_{\mathrm{gap}} \approx 0.0142\ \mathrm{MeV}. \tag{A5}$$

The two-state model predicts

$$E_{\mathrm{gap}} = |2mx_c| = 0.0164\ \mathrm{MeV} \tag{A6}$$

which agrees well with (A5).

Thus the two-state model seems to be very successful in estimating the properties of crossing singularities, at least in this particular case.

---

*Work supported in Part by the National Science Foundation.

†Work supported in part by the U. S. Energy Research and Development Administration.

[1]B. R. Barrett and M. W. Kirson, *Advances in Nuclear Physics*, edited by M. Baranger and E. W. Vogt (Plenum Press, N. Y.-London, 1973), Vol. 6.

[2]T. H. Schucan and H. A. Weidenmüller, Ann. Phys. (N. Y.) 73, 108 (1972); 76, 483 (1973).

[3]C. Bloch and J. Horowitz, Nucl. Phys. 8, 91 (1958).

[4]T. Morita, Progr. Theor. Phys. (Kyoto) 29, 351 (1963).

[5]B. H. Brandow, Rev. Mod. Phys. 39, 771 (1967).

[6]M. B. Johnson and M. Baranger, Ann. Phys. (N. Y.) 62, 171 (1971); T. T. S. Kuo, S. Y. Lee, and K. F. Ratcliff, Nucl. Phys. A176, 65 (1971); G. Oberlechner, F. Owono-N'-Gyema, and J. Richert, Nuovo Cimento B68, 23 (1970).

[7]I. Lindgren, J. Phys. B 7, 2441 (1974).

[8]M. Baranger, in *Nuclear Structure and Nuclear Reactions, Proceedings of the International School of Physics, "Enrico Fermi," Course XL, 1967*, edited by M. Jean and R. Rizzi (Academic, New York, 1969).

[9]B. R. Barrett, Nucl. Phys. A221, 299 (1974).

[10]T. T. S. Kuo and G. E. Brown, Nucl. Phys. 85, 40 (1966).

[11]B. R. Barrett and M. W. Kirson, Phys. Lett. 27B, 544 (1968); 30B, 8 (1969); Nucl. Phys. A148, 145 (1970).

[12]P. Goode, Phys. Lett. 51B, 429 (1974).

[13]P. A. Schaefer, Ann. Phys. (N. Y.) 87, 375 (1974); P. J. Ellis and E. Osnes, Phys. Lett. 45B, 425 (1973).

[14]P. J. Ellis and T. Engeland, Nucl. Phys. A144, 161 (1970); A181, 368 (1972); H. T. Fortune and S. C. Headley, Phys. Lett. 51B, 136 (1974).

[15]This subject is summarized by D. W. Sprung, in *Lecture Notes in Physics, Vol. 40, Effective Interactions and Operators in Nuclei*, edited by B. R. Barrett (Springer-Verlag, Berlin, Heidelberg, New York, 1975), p. 207.

[16]H. M. Hofmann, S. Y. Lee, J. Richert, H. A. Weidenmüller, and T. H. Schucan, Phys.Lett. 45B, 421 (1973); Ann. Phys. (N. Y.) 85, 410 (1974); H. M. Hofmann, J. Richert, and T. H. Schucan, Z. Phys. 268, 293 (1974).

[17]T.-S. H. Lee and S. Pittel, Phys. Lett. 53B, 409 (1975).

[18]E. M. Krenciglowa, T. T. S. Kuo, E. Osnes, and B. Giraud, Phys. Lett. 47B, 322 (1973); M. R. Anastasio, J. W. Hockert, and T. T. S. Kuo, *ibid.* 53B, 221 (1974); M. R. Anastasio, T. T. S. Kuo, and J. B. McGrory, *ibid.* 57B, 1 (1975).

[19]C. M. Vincent and S. Pittel, Phys. Lett. 47B, 327 (1973).

[20]N. Lo Iudice, D. J. Rowe, and S. S. M. Wong, Phys. Lett. 37B, 44 (1971); Nucl. Phys. A219, 171 (1974).

[21]B. R. Barrett, E. C. Halbert, and J. B. McGrory, Ann. Phys. (N. Y.) 90, 321 (1975).

[22]M. W. Kirson, in *Lecture Notes in Physics, Vol. 40, Effective Interactions and Operators in Nuclei* (see Ref. 15), p. 330.

[23]R. J. Eden and N. C. Francis, Phys. Rev. 97, 1366 (1955).

[24]H. A. Mavromatis, Nucl. Phys. A206, 477 (1973).

[25]P. Goode (unpublished).

[26]P. J. Ellis, Phys. Lett. 56B, 232 (1975).

[27]Y. Starkand and M. W. Kirson, Phys. Lett. 55B, 125 (1975).

[28]M. W. Kirson (private communication).

[29]G. A. Baker, Jr., *Advances in Theoretical Physics*, (Academic, New York, 1965), Vol. 1; J. Zinn-Justin, Phys. Rep. 1, 55 (1971).

[30]H. M. Hofmann, Contribution to the International Topical Conference on Effective Interactions and Operators in Nuclei, University of Arizona, June 2-6, 1975 (unpublished).

[31]B. M. Spicer and J. M. Eisenberg, Nucl. Phys. 63, 520 (1965).

[32]P. Federman and S. Pittel, Phys. Rev. 186, 1106 (1969).

[33]T. T. S. Kuo and S. Y. Lee (unpublished); S. Y. Lee Ph. D. thesis, S. U. N. Y. at Stony Brook, 1972 (unpublished).

[34]H. M. Hofmann, Y. Starkand, and M. W. Kirson, Contribution to the International Topical Conference on Effective Interactions and Operators in Nuclei, University of Arizona, June 2-6, 1975 (unpublished).

[35]Y. Starkand and M. W. Kirson, Contribution to the International Topical Conference on Effective Interactions and Operators in Nuclei, University of Arizona, June 2-6, 1975 (unpublished).

[36]S. Y. Lee (private communication).

[37]B. H. Brandow, *Lectures in Theoretical Physics*, edited by K. T. Mahanthappa and W. E. Brittin, (Gordon and Breach, New York, 1969), Vol. 11B, p. 55.